Mapana – Journal of Sciences
2023, Vol. 22, No. 1, 53-70
ISSN 0975-3303 | https://doi.org/10.12723/mjs.64.4

The Bubbling Milky Way: An Overview of Infrared Bubbles in Our Galaxy

K. A. Anjali*, R. Arun†, Blesson Mathew*, and Sreeja S. Kartha*

Abstract

Infrared bubbles are cavity-like structures formed around OB-type star(s) or star clusters. They are detected primarily at mid-infrared wavelengths. They usually enclose ionized gas and hot dust composed of very small grains. A combination of the thermal pressure of the expanding HII region, powerful stellar winds, and radiation pressure associated with massive stars contribute to the formation of a bubble. Expanding bubbles could trigger star formation, either via the collect and collapse process or radiatively driven implosion. This can further provide a pathway for understanding the aspects related to triggered star formation. This article provides a brief overview of infrared bubbles, their association with the HII region, the massive and young stellar objects they enclose, and the mechanisms of triggered star formation when they expand to the interstellar medium. As a representative example, we present a multiwavelength investigation of the northern infrared bubble CN71. The physical environment of the bubble CN71 is investigated using *Spitzer* data. We have detected 29 Class I/II YSOs and 459 Class III YSOs by NIR-MIR photometric analysis. We have also detected the presence of 5 OB-type stars within the bubble boundary.

*Department of Physics and Electronics, CHRIST (Deemed to be University), Bangalore; anjali.ka@phy.christuniversity.in; blesson.mathew@christuniversity.in; sreeja.kartha@christuniversity.in
†Indian Institute of Astrophysics, Bangalore; arunroyon@gmail.com

Using the Gaia EDR3, we estimated the distance to the bubble to be 1.6 kpc. Our preliminary analysis suggests that CN71 shows the signature of triggered star formation.

ISM: bubbles — ISM: clouds — stars: formation — ISM: HII region

1. Introduction

High-mass stars ($M \geq 8M_{\odot}$) impart notable consequences on their ambient medium because of their radiative, chemical, and mechanical feedbacks, form HII regions around them (Zinnecker & Yorke 2007). Due to their energetic stellar wind and UV radiation, they ionize and destroy parent molecular clouds, which ultimately results in the formation of cavity-like structures around them. These ubiquitous cavity-like structures in the Milky Way are referred to as bubbles (Churchwell et al. 2006, 2007; Dewangan et al. 2012, 2020; Baug et al. 2019; Kohno et al. 2021).

Galactic Legacy Infrared Survey Extraordinaire (GLIMPSE; Benjamin et al. 2003) by Spitzer Space Telescope produced high-resolution images at the mid-infrared wavelength (3.6 to 8.0 μm) of the galactic mid-plane. Churchwell et al. (2006, 2007) examined the GLIMPSE images and identified 600 parsec-scale mid-infrared (MIR) Galactic bubbles between the longitudes from -60° to +60°. In the visual inspection, bubbles are observed as full or partial rings which is a two-dimensional projection of a three-dimensional bubble. Bubbles are bordered by a photodissociation region and usually enclose ionized gas and hot dust. Later, Simpson et al. (2012), in their 'Milky Way Project' created an extended catalog of 5106 IR bubbles. Most of these bubbles show spatial association with HII regions, and many show morphological features that favor triggered or sequential star formation. In recent years, several bubbles have been recognized as potential zones for triggered star formation. However, a detailed analysis of such bubbles is needed to understand the role of other star formation processes, in addition to the contribution from triggered star formation (Kendrew et al. 2012).

This article aims to provide a concise introduction to MIR bubble research, with a specific analysis of the IR bubble CN71. The structure of the article is as follows. The formation of massive stars

and their various pressure components are discussed in Section 2. In Section 3, we describe the bubble morphology. Section 4 explores the importance of studying bubbles and possible scenarios of triggered star formation associated with the bubbles. In Section 5, we report some effective ways to identify young stellar objects and exciting star candidates associated with the bubbles, and Section 6 on the distribution of bubbles in the Galactic disk.

2. Formation of massive stars

Star formation in galaxies is a complicated process that involves many diverse physical processes such as radiation pressure, magnetic field, and protostellar outflows. High-mass star formation cannot be considered as a simple scaled-up version of low-mass star formation, and a complete picture of their formation is still unresolved. The problem is fundamental to astrophysics as it can dictate the evolution of a galaxy. The difficulty in decoding the whole star formation processes is due to relatively larger distances to the sources, high extinction of the Galactic disk, and short timescales of various evolutionary phases. In order to explain the formation of high-mass stars, three proposed scenarios are mentioned in the literature, and they are i) Core Accretion, ii) Competitive Accretion, and iii) Protostellar Collisions (Zinnecker & Yorke 2007; Tan et al. 2014). Let us look at each of these mechanisms in detail.

According to the *Core Accretion* model, gravitationally bound, centrally concentrated cores are the initial conditions required to form a high-mass star. These cores accrete materials from their surroundings, after which they undergo gravitational collapse via a central disk, resulting in the formation of a single star or a large number of small multiple systems (Shu et al. 1987; Tan et al. 2014). Initial conditions for the *Competitive Accretion* model are massive, gravitationally bounded star-less cores. Due to high turbulence, the materials that constitute a massive star are pulled in from a wider region of the clump (Tan et al. 2014). Massive stars may also form via *Protostellar Collisions* if the stellar density is very high near the cluster center (Tan et al. 2014). Detailed discussion and recent development of these concepts are given in the reviews of Bonnell & Bate (2002), Zinnecker & Yorke (2007), and Murray & Chang (2012).

There are at least two major distinctions between the low and high-mass star formation process. Firstly, the Kelvin-Helmholtz time scale of a high-mass star is smaller than the accretion time, due to which they start nuclear burning while accreting. Secondly, high-mass protostars tend to form in large enough dense cores so that the internal turbulence can dominate thermal motions (McKee & Ostriker 2007; Tan et al. 2014).

2.1 Pressure effects of massive stars

The rapid evolution of massive stars has a prompt effect on the immediate environment. We discuss some of the pressure effects of massive stars affecting the nearby regions. These pressure effects are due to stellar wind (P_{wind}), radiation (P_{rad}), and ionized gas (P_{HII}). The pressure owing to the stellar wind (P_{wind}) is given by the expression:

$$P_{wind} = \frac{M_w V_w}{4\pi D_s^2}$$

where M_w is the mass loss rate, V_w is the stellar wind velocity, D_s is the stellar distance (Baug et al. 2019, Arun et al. 2021). The pressure component due to radiation (P_{rad}) can be calculated using the equation:

$$P_{rad} = \frac{L_{bol}}{4\pi D_s^2}$$

where L_{bol} is the bolometric luminosity. The ionized gas pressure (P_{HII}) can be calculated using the equation:

$$P_{HII} = \mu_{II} m_H c_{II}^2 \left(\frac{N_{Lyc}}{4\pi \beta_2 D_s^3} \right)^{1/2}$$

where μ_{II} is the mean molecular weight in an HII region, c_{II} is the speed of sound in an HII region, β_2 is the recombination coefficient, and S_{Lyc} is the Lyman continuum flux of the massive star (Dewangan et al. 2017; Baug et al. 2019; Arun et al. 2021).

In general, the expansion of the ionized gas is thought to be a major and efficient process that could trigger star formation. Hence, it is noteworthy to analyze and understand the pressure imparted by these HII regions (Baug et al. 2019).

3. Bubble Morphology

A comparison of catalogs of known HII regions and catalogs of star clusters clearly indicates the association of IR bubbles with the HII regions. Literature tells us that around 86% of bubbles encompass known HII regions (Zavango et al. 2006; Deharveng et al. 2010; Ji et al. 2012; Beaumont et al. 2014; Zhou et al. 2020). So, bubbles can be considered as HII regions that enclose massive star(s) or a star cluster. Figure 1 shows a simple model of HII region formation and evolution in a uniform homogeneous medium. Two major phases can be used to dictate the life of an HII region. First, a short formation phase, is followed by a long expansion phase. During the formation phase, the central star(s) expeditiously ionizes its neutral surrounding, and a high-pressure region of ionized gas and a low-pressure region of cold neutral medium will be created. Due to the existence of this pressure gradient, the HII region starts to expand, which is called the expansion phase. During this supersonic expansion of the HII region, neutral material collects between the ionization front (IF) and the shock front (SF). This swept-up layer of neutral materials and cold dust around the ionized region of hot gas and dust becomes very massive with time, which may result in the formation of a new generation of stars in the collected layer (Beaumont et al. 2014). The mass of the swept-up layer and its formation time scale varies with the ionizing photon flux of the central star and its ambient gas density. The typical time scale for layer fformation could be less than 1 Myr. When the density of this layer reaches 10-100 times of ambient gas density and mass reaches thousands of $M_{\odot}$, gravitational fragmentation is expected. Small-scale gravitational instabilities result in the formation of low-mass stars in the collected layer, while large-scale instabilities result in the formation of massive fragments, where massive stars can form (Hosokawa & Inutsuka 2006).

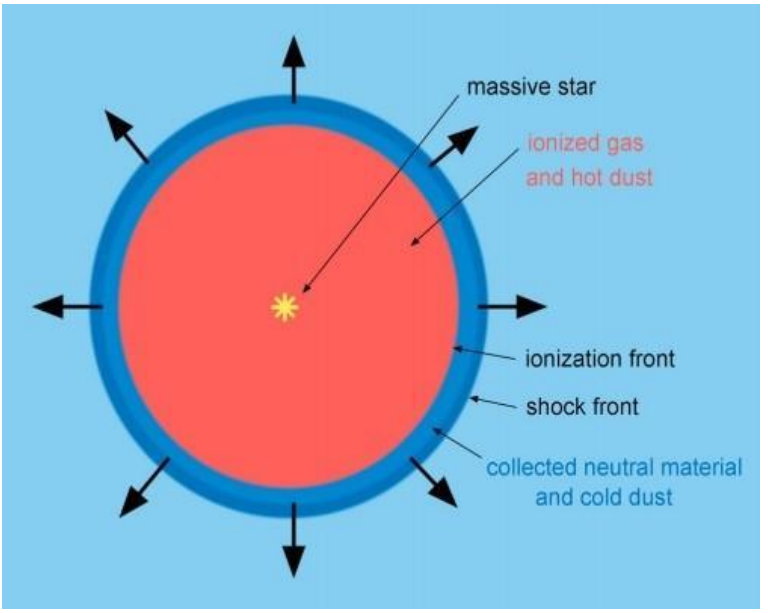

Figure 1: A simple model of HII region expansion in a uniform homogeneous medium. The ionized region of gas and hot dust is surrounded by a shell of dense neutral material collected between IF and SF during the expansion phase. Figure adapted from Deharveng et al. (2010).

3.1 Bubbles observed by Spitzer

Inclusive and statistical study of bubbles in the Milky Way can be done with the help of the *Spitzer Space Telescope* and its surveys of inner galactic midplane - GLIMPSE (Benjamin et al. 2003) and MIPSGAL (Carey et al. 2009). Since the galactic disk is characterized by high extinction, mid-infrared wavelengths are appropriate for bubble observations, as they can emerge from the embedded regions in the Galactic disk. Figure 2 shows the *Spitzer* colour composite image of the region towards bubble CN71, which has not been studied individually yet. CN71 is a northern IR bubble that is centered at a_{2000} = 270.19867°, δ_{2000} = -24.09447°. It has an effective radius of 5.45 arcminute (Churchwell et al. 2006). The bubble's boundary is most noticeable in the GLIMPSE 8μm band. Emission at this wavelength is due to polycyclic aromatic hydrocarbon (PAH) molecules. PAHs are excellent at defining the photodissociation regions (PDRs), as they get destroyed by UV radiation in the ionized region. PDRs are peripheries of molecular clouds illumed by high-energy UV photons from the massive

central star(s). PAHs get excited due to high energy UV photons which permeate the PDRs, resulting in an 8μm emission, which defines the bubble boundary (Watson et al. 2008, 2010; Deharveng et al. 2009; Sidorin et al. 2014; Cappa et al. 2017). So, bubbles can be considered ideal objects to explore and understand the effects of UV radiation produced by the central star(s) on its parent molecular cloud.

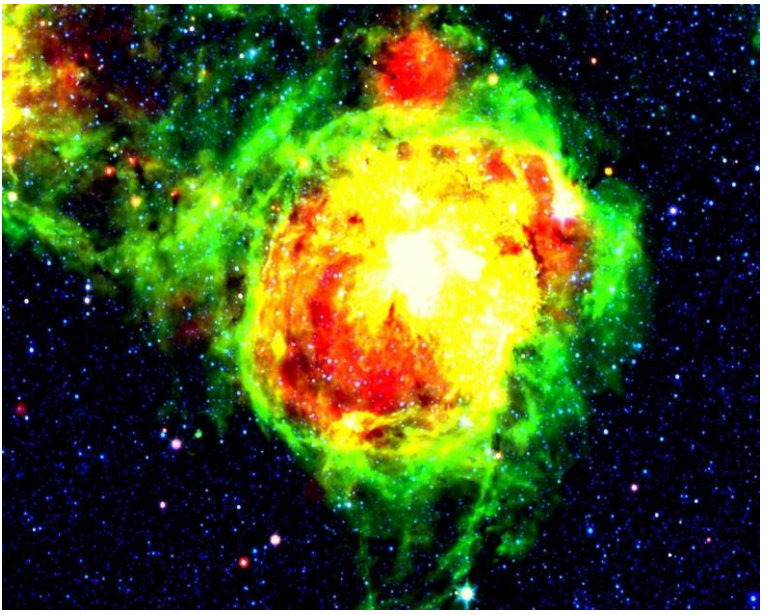

Figure 2: The *Spitzer* colour composite image of the region towards bubble CN71. Red corresponds to the 24μm emission, green to the 8μm emission, and blue to the 4.5μm emission. Yellow and white correspond to the region where emissions in three bands are intense.

Emission at 24μm was observed in the Multiband Imaging Photometer for Spitzer (MIPS) that fills the bubble's cavity, contrary to the 8μm continuum, which traces the bubble rim/boundary. The 24μm emission is observed mainly in two locations: first, towards the center of the bubble and towards the border. Emission at this wavelength is due to very small grains (VSGs) having sizes in the range of 1 nm to 10 nm. These VSGs heat up by absorbing high-energy photons from the central star(s) and radiate in the near- and mid-IR wavelengths. The 24μm traces from the center can be exploited to locate the central star(s) within the bubble PDR (Deharveng et al. 2010; Petrella et al. 2010; Zhang et al.

2012; Liu et al. 2016). The emission at 4.5μm shows mostly the point sources in the Spitzer image. The 24μm emission at the top of the bubble beyond the bubble boundary can possibly be young stellar objects (YSOs) projected on the bubble periphery but not a secondary bubble (Churchwell et al. 2007). In conclusion, MIR color-composite image reveals the morphology and extension of bubbles. Naturally, one might wonder and ask what is the necessity to study bubbles. Let us now discuss in brief the importance of studying infrared bubbles.

4. Importance of studying bubbles

First, MIR bubbles are ideal laboratories to investigate the effect of young, hot, massive OB stars or star clusters on their surrounding ISM. Feedback from the massive central star(s) ionizes and heats the gas and dust around them. As a consequence of this, bubbles/HII regions expand. So, infrared dust bubbles are promising objects to study the interplay between PDR and cold molecular gas and the structure. IR bubbles can also provide crucial pieces of information about the physical and structural properties of ISM in which they expand (Deharveng et al. 2010).

Secondly, the characteristic morphology and extension of a bubble are mainly determined by the luminosity, wind strength, and motion relative to the ambient ISM of the central star which creates the bubble. Another factor that influences bubble morphology is the density of the surrounding ISM. Hence, vital information regarding the directionality and strength of the stellar wind can be derived from bubble morphology. Certain bubbles exhibit extra growths from their boundaries, often appearing as pillars and globules in 8μm emission. These structures provide unique information about hydrodynamics, photoionization, evaporation of gas and sublimation of dust in expanding bubbles, and stellar mass loss rates (Watson et al. 2008).

Thirdly, MIR bubbles are the testbeds to study triggered star formation mechanisms. Recently, several IR bubbles which enclose expanding HII regions have been defined as potential zones to investigate the signature of triggered/sequential star formation (Devangan et al. 2017; Liu et al. 2015; Baug et al. 2018).

4.1. Triggered star formation: Possible scenarios

When the feedback from various energetic events induces/triggers the formation of the next generation of stars, it is called triggered or sequential star formation. Proposed energetic events which trigger star formation involve supernova explosions, high-mass star formation, cluster formation, energetic winds of massive stars, protostellar outflow, spiral density waves, and galaxy-galaxy interactions (on Galactic scales). Triggered star formation is considered an effective self-sustained mechanism shown by galaxies through which the next generation of stars are formed (Elmegreen et al. 2011).

Two commonly proposed scenarios for triggered star formation in literature are the *Collect and Collapse* (CC) process and *Radiatively Driven Implosion* (RDI). According to Elmegreen & Lada (1977), during the CC process, neutral gas gets collected and compressed between ionizing and shock fronts of expanding HII region. Swept-up mass then fragments and collapses to create massive fragments (of the order of $7M_{\odot}$; Elmegreen et al. 1998; Kendrew et al. 2012). Recent years have witnessed a plethora of studies on the boundaries of known star-forming regions to exploit the CC process, using observations as well as simulations (Deharveng et al. 2005).

Radiatively driven implosion (RDI) is thought to act on smaller spatial scales whilst the CC process acts on larger scales along the bubble boundary. RDI occurs when the ionized gas pressure component (P_{HII}) of a young massive star compresses and collapses the pre-existing clumpy cloud core, often in the form of narrow pillars, globules, or cometary shapes. A clumpy cloud core radiatively implodes, forming a new generation of stars. The time scale of RDI mainly depends on two factors. First, the ionization flux of a massive star and the time required for pressure disturbance to reach the clump. RDI often results in the formation of low and intermediate-mass stars. Observational evidence of RDI around OB associations and edges of relatively old HII regions further confirms this (Mitoyama et al. 2006).

A solid positional correlation between YSOs and HII regions is evident from the Milky Way Project (Simpson et al. 2012). A

statistically significantly higher number of young sources associated with bubbles that encompass expanding HII region indicates an ongoing star formation process.

5. Search for associated YSOs and Exciting Stars

The presence of YSOs towards the region of MIR bubbles is apparent from various studies, although their formation might not always be due to the triggered star formation mechanism. The YSO distribution in and around the bubble provides some key signs of star formation. Potential YSOs can be classified by Lada et al. (1987) into 3 categories:

i) Class I – Protostars

ii) Class II - Pre-main sequence stars with disk

iii) Class III - Main sequence stars and debris disk objects

YSOs associated with the molecular clouds can be classified into different classes based on the IRAC color selection scheme proposed by Gutermuth et al. (2009), using Spitzer IRAC band magnitudes ([3.6],[4.5],[5.8],[8.0]), which were used in several studies (Baug et al. 2016; Li et al. 2018).

Another efficient YSO identification method is Allen's classification scheme using IRAC colors (Allen et al. 2004; Das et al. 2016; Cappa et al. 2016). According to Lada et al. (1987), YSOs can be classified based on their spectral index value of SED. Spectral index (a) can be calculated (Lada et al. 1987; Wilking et al. 1989; Greene et al. 1994) as:

$$\alpha = \frac{d\log(\lambda F_\lambda)}{d\log(\lambda)}$$

Source falls into Class I if $0 < a \leq +3$, source falls into Class II if $-2 < a \leq 0$, and source falls into Class III if $-3 < a \leq -2$ (Lada et al. 1987; Das et al. 2017; Li et al. 2018). Also, the JHK_s[3.6][4.5] YSO classification scheme proposed by Gutermuth et al. (2008) has been efficiently used by various authors for the classification of YSOs (Ojha et al. 2004a, b; Petrilla et al. 2010; Dewangan et al. 2016, 2018).

YSO distribution overlayed onto spitzer color composite image gives some insight into the triggered star formation mechanism. A

good spatial correspondence between the two suggests triggered star formation.

Bubbles must be formed by O and/ or B-type stars as they are evidently associated with HII regions (Churchwell et al. 2006, 2007). Taking the proper motion of ionizing sources into consideration, we cannot expect them to locate at the geometrical center of the bubble always. However, bubbles are young objects, and ionizing sources may not get enough time to cross and go beyond bubble boundaries (Petrilla et al. 2010). So, massive star(s) located within the PDR of the bubble can be considered as the exciting candidate(s) which create the bubble.

As the main sequence stars belong to Class III, the ionizing sources can be searched among Class III sources. Based on the position of the object in the K_s versus *(J-H)* color-magnitude diagram (CMD) and K_s versus $(H-K_s)$ CMD, the object can be a main sequence star and its spectral type can be O or B, respectively (Petrilla et al. 2010; Cappa et al. 2016).

Another effective method for identification of exciting star(s) is the *BJHK* color criteria of Comer´on & Pasquali (2012), which are used by several studies as it can effectively sort and remove low-mass stars (Ortega et al. 2016; Das et al. 2017). As an additional constraint on the search for ionizing stars, the SED of the selected candidates can be plotted. The effective temperature derived from SED should be consistent with the temperature of O- and B- type stars (Petrilla et al. 2010). Candidate satisfying all of the above criteria simultaneously plotted over 8μm image gives the exciting stars within the PDR of the bubble. Among the aforementioned methods, we use JHK_s[3.6][4.5] YSO classification scheme proposed by Gutermuth et al. (2008) to identify YSOs and BJHK color criteria of Comer´on & Pasquali (2012) to identify exciting candidates associated with CN71, which is discussed in detail in the next section.

5.1. Stellar population associated with the IR bubble CN71

A thorough analysis of the literature revealed that the IR bubble CN71 has not been the subject of any legitimate individual studies. So, identifying YSOs and exciting candidates associated with CN71 is what we are attempting to do here.

To identify the YSOs associated with the IR bubble CN71, and hence to study the star formation activity associated with the bubble, we extracted the 2MASS and GLIMPSE II Spring'08 data of the stars in a region 1.5 times the bubble radius. To obtain stars with good-quality data, we retain sources with the 2MASS quality flag 'AAA'. Of these sources, those with 3.6 and 4.5 IRAC magnitude ([3.6] and [4.5]) uncertainty < 0.1 mag are used for further analysis. We use the method proposed by Gutermuth et al. (2008) using JHKs and [3.6], [4.5] magnitudes for the identification of YSOs. Figure 3 shows the ([3.6]-[4.5]) versus (Ks-[3.6]) IR colour-colour diagram (CCD). Following the JHKs[3.6][4.5] YSO classification scheme, we have identified 29 Class I/II YSOs and 459 Class III YSOs. The possibility of triggered star formation in the region towards the bubble CN71 is suggested by a statistically significant number of YSOs around the bubble boundary.

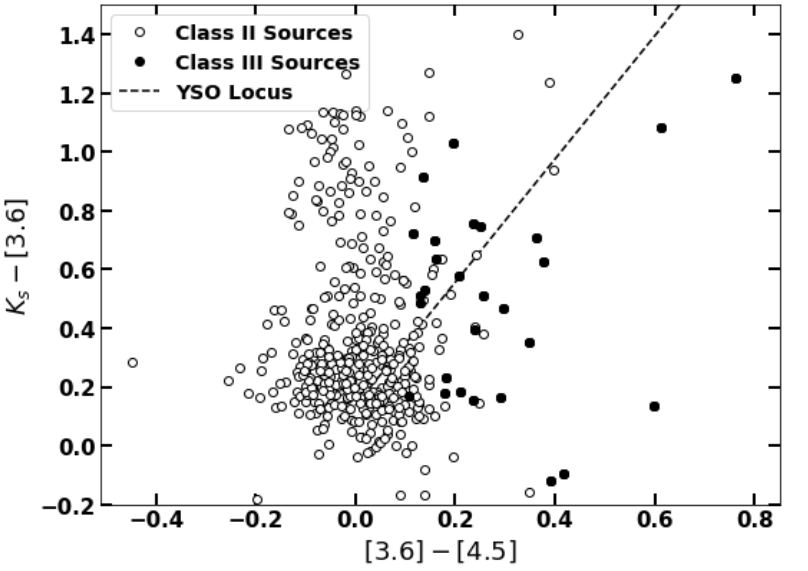

Figure 3: ([3.6]-[4.5]) versus (*Ks*-[3.6]) CCD of objects within the PDR of northern IR bubble CN71. Class III sources are represented as black circles. The black filled circle represents Class I/II sources.

We use the highly efficient *BJHK* color criteria of Comer´on & Pasquali (2012) to search ionizing sources within the PDR of the bubble CN71. For this, B magnitudes are retrieved from the

NOMD1 catalog. Index cuts, $Q_{BJK} = 0.196(B-J) - 0.981(J-K) - 0.098 > 0$ and $Q_{JHK} = 0.447(J-H) - 0.894(H-K) - 0.089 < 0$ are most efficient in eliminating late-type contaminants. Using this method, we identify 5 sources as potential exciting candidates. To further confirm the result, spectroscopic examination of these candidates is required. Figure 4 displays the distribution of potential exciting stars (green star) and Class I/II YSOs (red star) over the *Spitzer* color composite image of the bubble CN71.

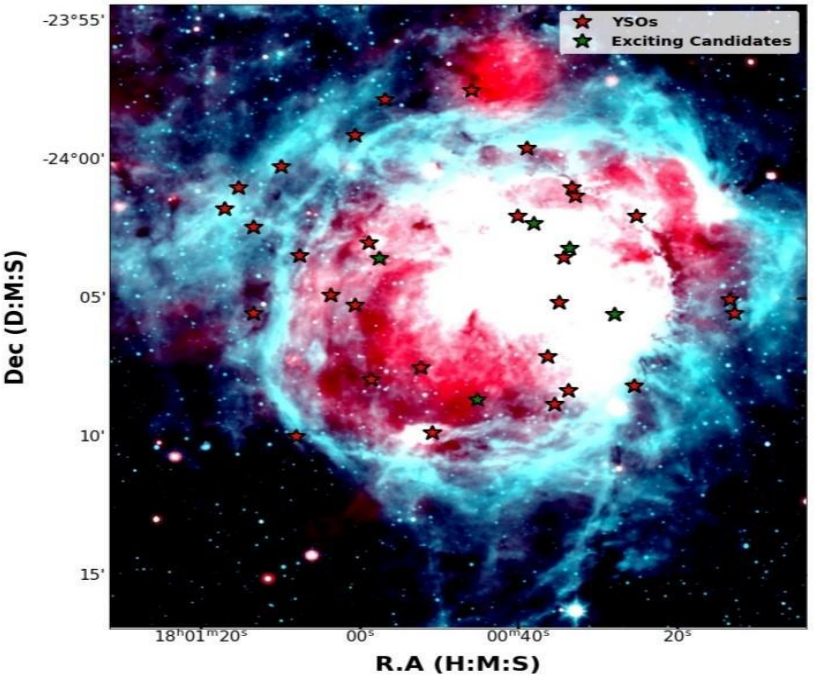

Figure 4: This figure displays the distribution of potential exciting stars (green star) and Class I/II YSOs (red star) over the *Spitzer* colour composite image of the bubble CN71. Red corresponds to the 24μm emission, and turquoise to the 8μm emission.

6. The Bubbling Galactic Disk

According to Churchwell et al. (2006, 2007), each square degree of the GLIMPSE survey area contains 1.5 bubbles on average and these bubbles are concentrated towards the Galactic midplane. Due to numerous limits in the visual investigation of the GLIMPSE survey region, both Churchwell's catalog (Churchwell et al. 2006) and Simpson's catalog (Simpson et al. 2012) of bubbles are

incomplete. For example, it is very challenging to distinguish bubbles from the visual search that subtends extremely small and very big solid angles. Furthermore, background and foreground emissions make the search more challenging. Figure 5 shows the distribution of IR bubbles in the Galactic disk. The presence of 59% of bubbles in the southern half of the plane clearly shows the asymmetry in the distribution of IR bubbles on both sides of the Galactic mid-plane (Churchwell et al. 2006). If we relate this asymmetry in the bubble distribution with the already existing fact that the number of molecular clouds in the southern half is more than that in the northern half (Dame et al. 1987), the association of young O and B stars with the bubbles is clear. So, studying the overall distribution of the bubbles is the key to understanding the global star formation trend in Milky Way. Probing YSOs and ionizing stars associated with the bubble is an efficient way to estimate the distance to the bubble as much as it is effective in studying the triggered star formation mechanism. Using the photogeometric distance values from Gaia EDR3 (Bailer-Jones et al. 2020), the median distance of the YSOs and the exciting candidates is estimated as 1.6 kpc. This can ideally be taken as the mean distance to the bubble from the Earth. Thus, a global and precise distance estimate of IR bubbles can be done from future Gaia data releases.

Figure 5: This figure shows the distribution of IR bubbles in the Galactic disk. The bubbles identified by Churchwell et al. (2006) are shown in red, and those identified by Simpson et al. (2012) through 'The Milky Way Project' are shown in blue.

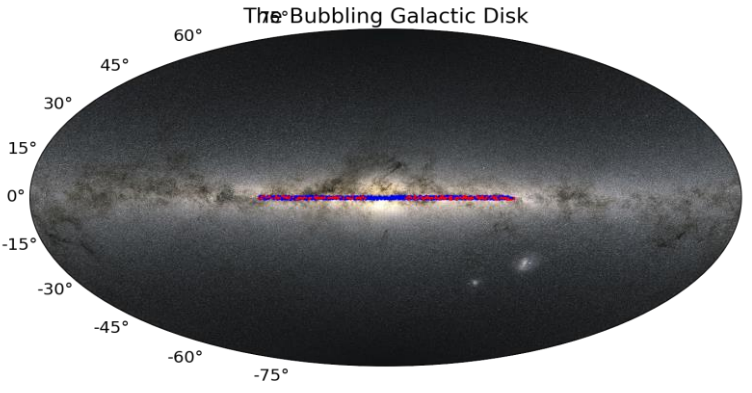

7. Conclusion

In this article, we provide an introduction to MIR bubbles, their morphologies, the HII region they enclose, and the associated massive star and YSO population. We also discuss the triggered star formation process and its possible scenarios associated with bubbles using the information available from the works done to date in bubbles.

Bubbles are cavity-like structures formed around OB-type star(s) or star clusters, detected mainly at mid-infrared wavelength, which usually encloses ionized gas and hot dust. In the MIR color composite image, the bubble boundary is most visible in the 8μm maps, which feature PAH molecules. Continuum emission at 24μm, which fills the bubble's cavity, is due to very small warm dust and UV irradiating stars. IR bubbles enclosing the expanding HII regions are recognized as potential sites to study the signature of triggered star formation. Statistically significant overdensity of YSOs around bubble rim implicates triggered star formation. Identification of ionizing/exciting sources and their spectral type helps to further confirm the triggered star formation mechanism.

CN71 is a less studied northern IR bubble which is centered at α_{2000} = 270.19867°, δ_{2000} = -24.09447° with an effective radius of 5.45 arcminute. Within the bubble PDR, we identified 5 stars as potential exciting candidates which create the bubble, using optical and NIR colors. From NIR and IRAC colors, we identified 29 Class I/II YSOs and 459 Class III YSOs within the PDR of the bubble CN71. Statistically significant overdensities of YSOs associated with the bubbles indicate that this region is a site of recent star formation activities. From the Gaia data, we estimated the distance to the bubble from the Earth as 1.6 kpc, suggesting that this is a nearby bubble as the calculated distance is less than 2 kpc.

While precise proper motion data from *Gaia* could help to identify exciting stars more accurately, future MIR observations using the *James Web Space Telescope* could reveal vital information about the deeply embedded young star population. These observations will definitely revolutionize the research field of IR bubbles.

References

[1] Allen L. E. et al., 2004, ApJS, 154, 363

[2] Arun, R., Mathew, B., Maheswar, G., et al. 2021, , 507, 267

[3] Baug, T., Dewangan, L. K., Ojha, D. K., et al. 2016, , 833, 85

[4] Baug T., de Grijs R., Dewangan L. K., Herczeg G. J., Ojha D. K., Wang K., Deng L., Bhatt B. C., 2019, ApJ, 885, 68

[5] Bailer-Jones C. A. L., Rybizki J., Fouesneau M., Demleitner M., Andrae R., 2020, AJ, 161, 24

[6] Beaumont, C. N., Goodman, A. A., Kendrew, S., et al. 2014, , 214, 3

[7] Benjamin R. A. et al., 2003, PASP, 115, 953

[8] Bonnell IA, Bate MR. 2002. MNRAS 336:659–669

[9] Cappa, C. E., Duronea, N. U., Vasquez, J., et al. 2016, arXiv:1611.02661

[10] Carey, S. J., Noriega-Crespo, A., Mizuno, D. R., et al. 2009, , 121, 76

[11] Churchwell E. et al., 2006, ApJ, 649, 759

[12] Churchwell, E., Watson, D. F., Povich, M. S., et al. 2007, , 670, 428.

[13] Comeron F., Pasquali A., 2012, AA, 543, A101

[14] Dame, T. M., et al. 1987, APJ, 322, 706

[15] Das, S. R., Tej, A., Vig, S., et al. 2017, , 472, 4750

[16] Deharveng, L., Zavagno, A., Caplan, J. 2005, AA, 433, 565

[17] Deharveng, L., Zavagno, A., Schuller, F., et al. 2009, , 496, 177

[18] Deharveng, L., Schuller, F., Anderson, L. D., et al.2010, , 523, A6

[19] Dewangan, L. K., Ojha, D. K., Anandarao, B. G., et al. 2012, , 756, 151

[20] Dewangan, L. K., Baug, T., Ojha, D. K., et al. 2016, , 826, 27

[21] Dewangan, L. K., Ojha, D. K., Zinchenko, I., et al. 2017, , 834, 22

[22] Dewangan, L. K., Baug, T., Ojha, D. K., et al. 2018, , 864, 54

[23] Dewangan, L. K.; Baug, T.; Pirogov, L. E.; Ojha, D. K.; 2020, ApJ, 898 , 41

[24] Duronea, N. U., Cappa, C. E., Bronfman, L., et al. 2017, , 606, A8 [25] Duronea, N. U., Cichowolski, S., Bronfman, L., et al. 2021, , 646, A103

[26] Elmegreen, B., Lada, C. 1977, ApJ, 214, 725

[27] Elmegreen, B. 1998, in Origins, ASP Conference Series vol. 148, ed. C. E. Woodward, J. Shull, H. Thronson, 150–183

[28] Elmegreen, B. 2011, in Ecole Evry Schatzman 2010: Starformation in the Local Universe, ed. C. Charbonnel T. Montmerle (EAS Publications Series), 1 – 16

[29] Greene, T. P., Wilking, B. A., Andre, P., Young, E. T., Lada, C. J. 1994 , ApJ, 434, 614

[30] Gutermuth R. A. et al., 2008, ApJ, 674, 336

[31] Gutermuth, R. A., Megeath, S. T., Myers, P. C., et al. 2009, ApJS, 184, 18

[32] Hosokawa, T., Inutsuka, S. 2006, ApJ, 648, L131

[33] Ji, W.-G., Zhou, J.-J., Esimbek, J., et al. 2012, , 544, A39

[34] Kendrew, S., Simpson, R., Bressert, E., et al. 2012, , 755, 71

[35] Kohno, M., Tachihara, K., Fujita, S., et al. 2021, 73, S338

[36] Lada C. J., 1987, in Peimbert M., Jugaku J., eds, IAU Symp. 115, Star Forming Regions. Kluwer, Dordrecht, p. 1

[37] Li, H., Li, J.-Z., Yuan, J.-H., et al. 2018, Research in Astronomy and

Astrophysics, 18, 122

[38] Liu, H.-L., Wu, Y., Li, J., et al. 2015, , 798, 30

[39] Liu, H.-L., Li, J.-Z., Wu, Y., et al. 2016, , 818, 95

[40] McKee C. F. and Ostriker E. C. (2007) Ann. Rev. Astron. Astrophys. 45 , 565

[41] Meyer M. R., Calvet N., Hillenbrand L. A., 1997, AJ, 114, 288

[42] Motoyama, K., Umemoto, T., & Shang, H. 2007, , 467, 657

[43] Murray N, Chang P. 2009. ApJ 746:75

[44] Ojha D. K. et al., 2004a, ApJ, 608, 797

[45] Ojha D. K. et al., 2004b, ApJ, 616, 1042

[46] Ortega, M. E., Giacani, E., Paron, S., et al. 2016, , 458, 3684

[47] Petriella, A., Paron, S., Giacani, E. 2010, , 513, A44

[48] Ranjan Das, S., Tej, A., Vig, S., et al. 2016, , 152, 152

[49] Shu F. H. et al. (1987) Ann. Rev. Astron. Astrophys., 25, 23

[50] Simpson, R. J., Povich, M. S., Kendrew, S., et al. 2012, 424, 2442

[51] Sidorin, V., Douglas, K. A., Palouˇs, J., et al. 2014, , 565, A6.

[52] Tan, J. C., Beltr´an, M. T., Caselli, P., et al. 2014, Protostars and Planets VI, 149.

[53] Watson, C., Povich, M. S., Churchwell, E. B., et al. 2008, , 681, 1341

[54] Watson, C., Hanspal, U., Mengistu, A. 2010, , 716, 1478

[55] Wilking, B. A. 1989, PASP, 101, 229

[56] Zavagno, A., Deharveng, L., Comer´on, F., et al. 2006, , 446, 171

[57] Zhang, C. P. Wang, J. J. 2012, 544, A11

[58] Zhang, C.-P. Wang, J.-J. 2013, Research in Astronomy and Astrophysics, 13, 47.

[59] Zinnecker H. and Yorke H. (2007) Ann. Rev. Astron. Astrophys. 45, 481